# Supplementary Figure 1

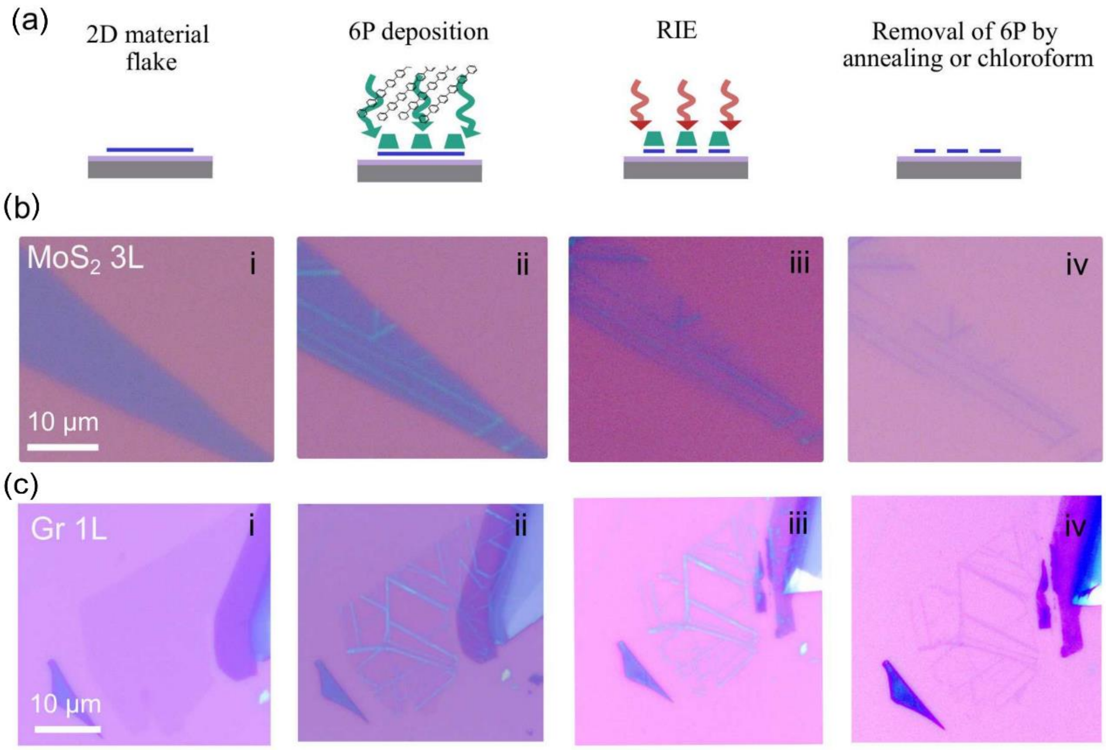


**Supplementary Figure 1**: Nanoribbon fabrication steps. (a) Schematics for the steps involved in the nanoribbon fabrication process. (b) and (c (i-iv)) shows the optical microscope images of the steps applied to a 3 layered (3L) $MoS_2$ and graphene monolayer. i) an exfoliated flake is transferred onto Si/$SiO_2$. ii) organic molecules are deposited via hot wall epitaxy process. iii) the flake is subjected to reactive ion etching with oxygen plasma. iv) nanoribbon network is annealed under high vacuum or rinsed in chloroform to remove the organic molecules.

# Supplementary Figure 2

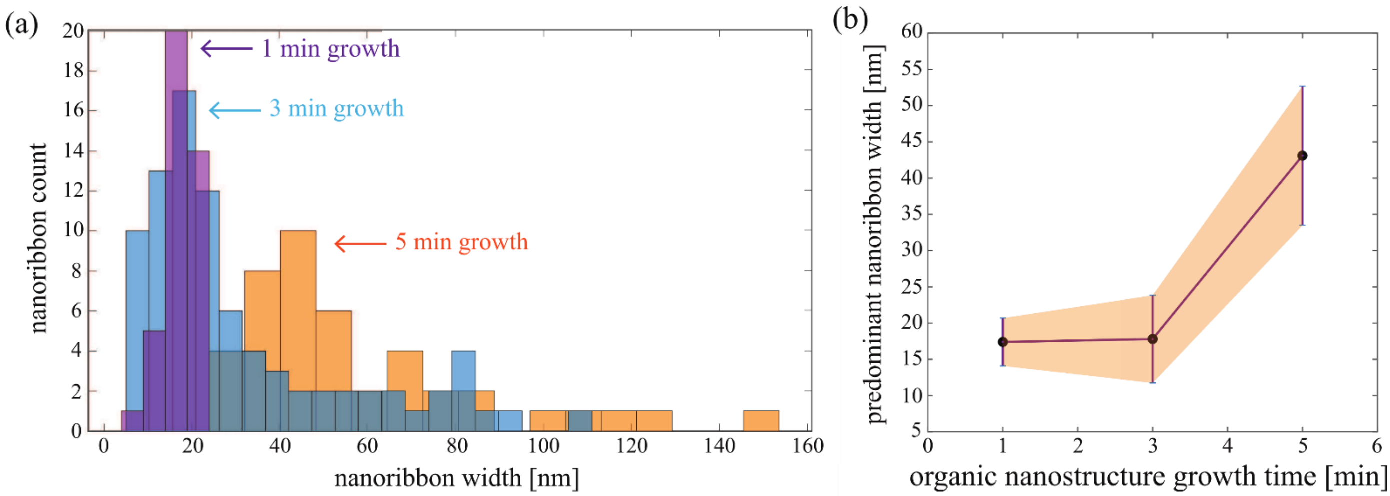


**Supplementary Figure 2**: Changes in the width of the nanoribbons via changing of the growth time of organic nanostructures. (a) presents the graphene nanoribbon width distributions when only the growth times of 6P on monolayer graphene flakes are altered (growth rate of 0.5 ML/min). Focusing on the main peaks in the histograms, extracted mean values and the standard deviations of the nanoribbon widths are provided as a function of the growth time in (b).

# Supplementary Figure 3

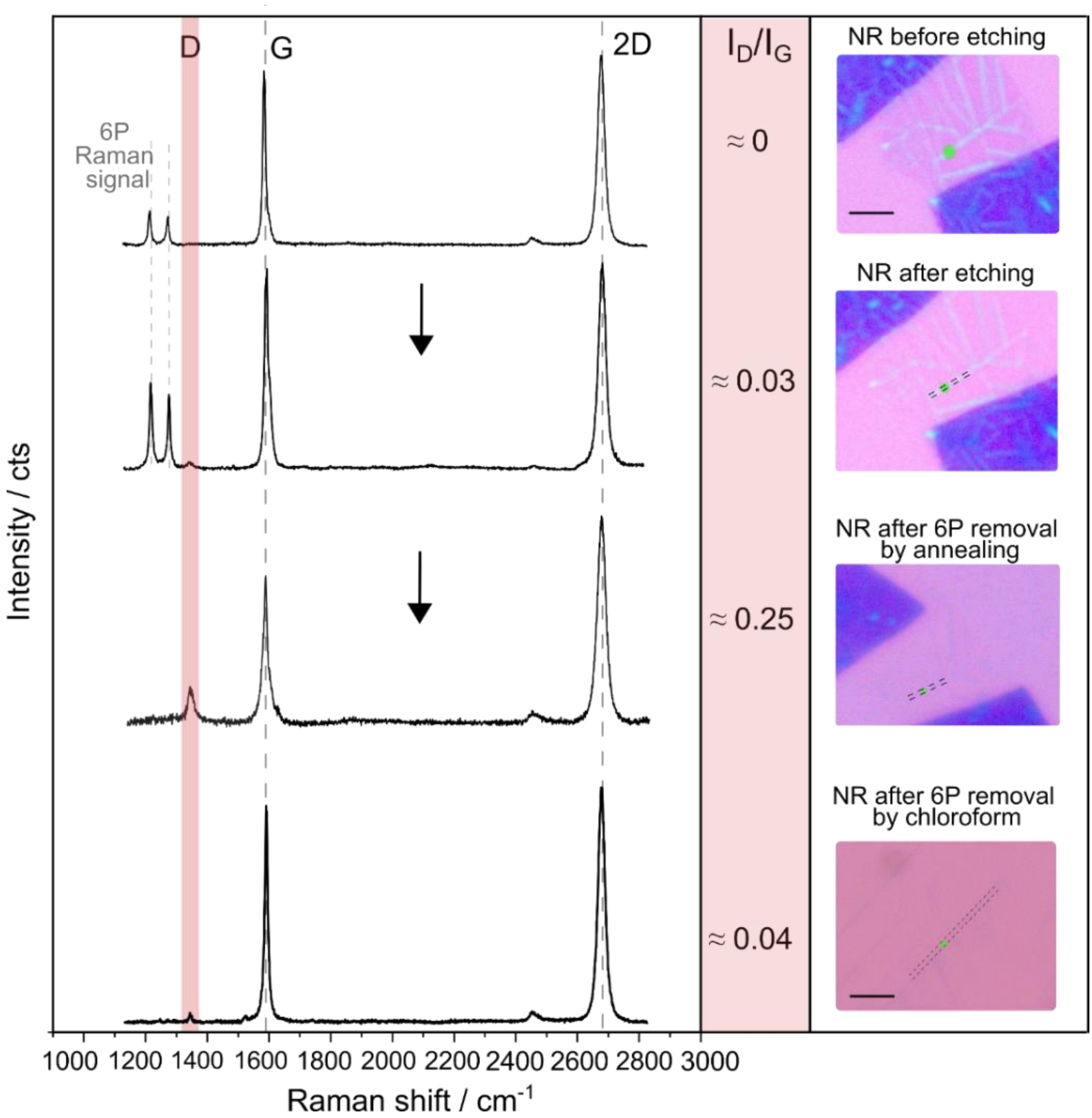


Supplementary Figure 3: Evolution of Raman spectra over various stages of graphene nanoribbon fabrication. The positions of the measurements are marked by a green dot on each optical image (sale bar 5 µm). Black dashed lines (on optical images) serve as a guide to the eye for the location of the measured ribbon. The first three presented spectra are measured on the same sample spot after each step, while the spectra for the NR after chloroform rinsing are shown for a different graphene NR sample following the same fabrication parameters, just without the annealing step.

# Supplementary Table 1

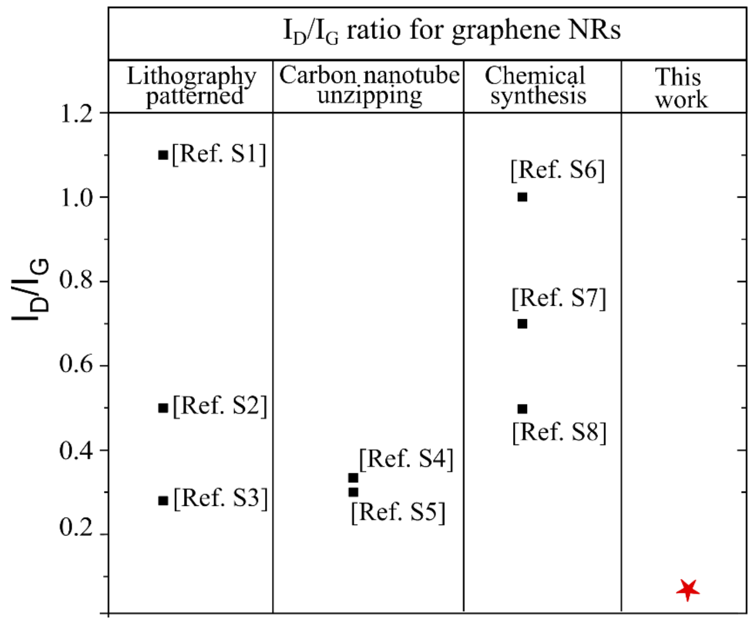


Supplementary Table 1: Comparison of $I_D/I_G$ peak ratios considering various strategies for fabrication of graphene nanoribbons. [S1-S8]

# Supplementary Figure 4

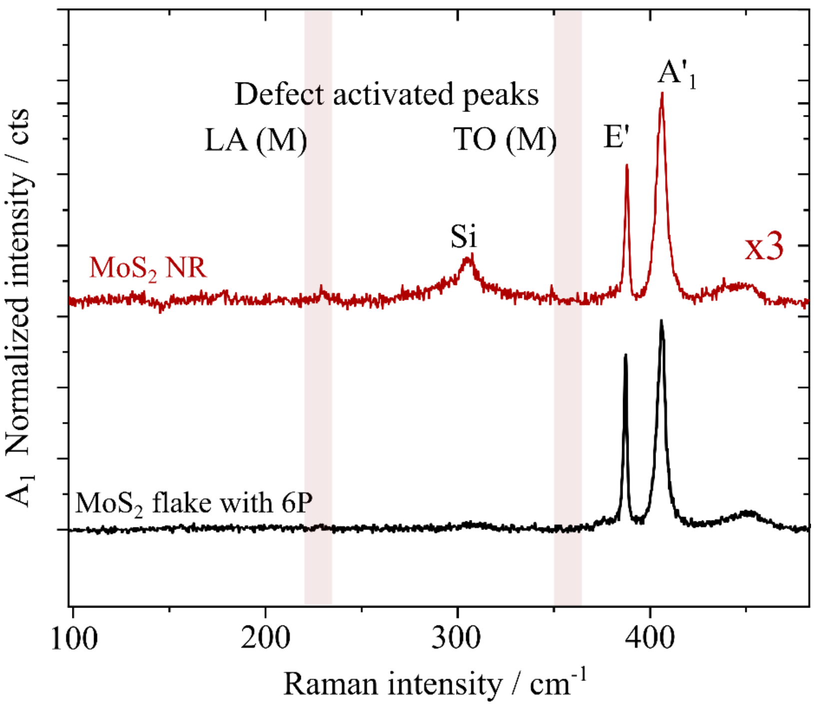


Supplementary Figure 4: shows the absence of defect related peaks in both, monolayer $MoS_2$ flake and the fabricated $MoS_2$ nanoribbon.

# Supplementary Figure 5

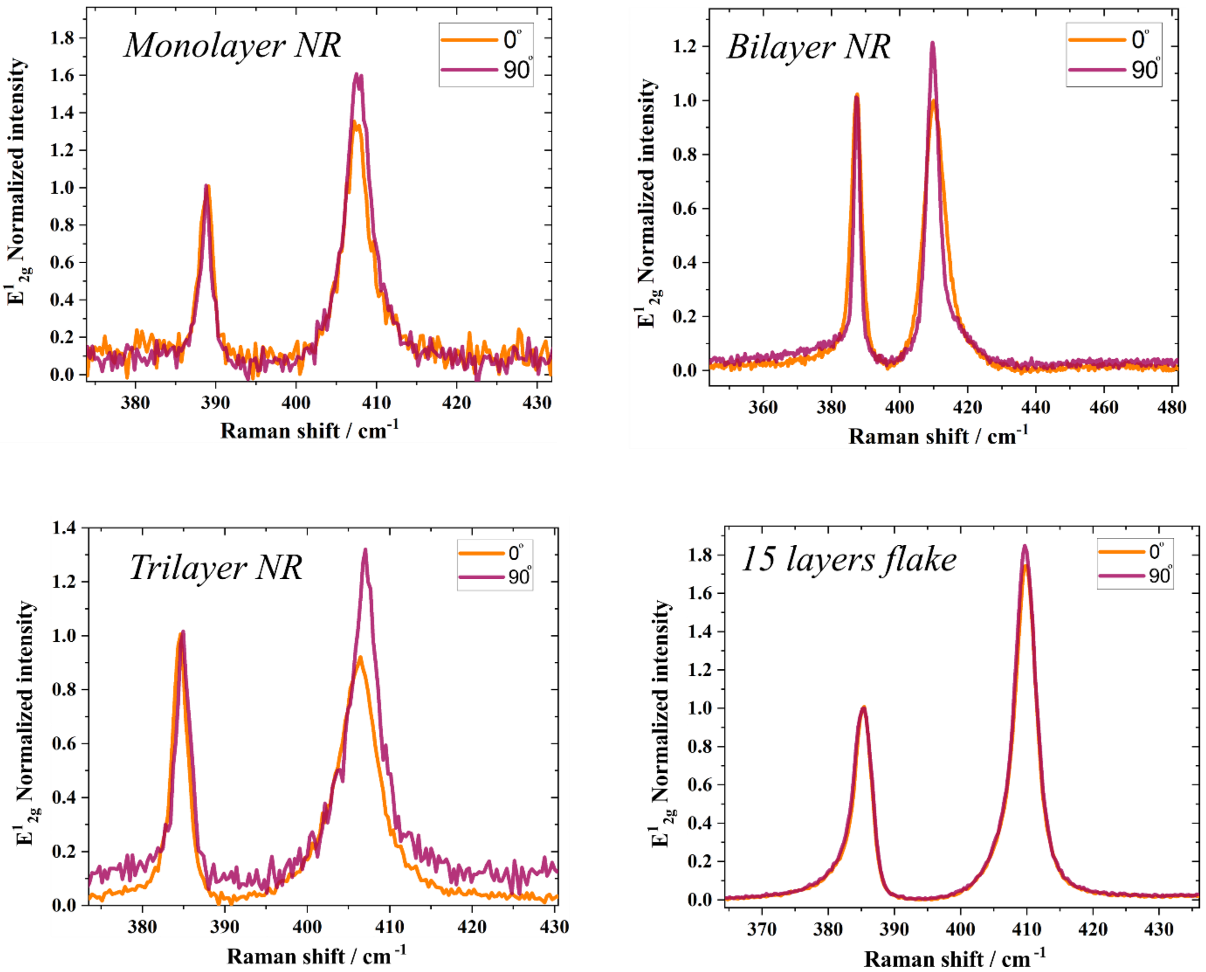


Supplementary Figure 5: Raman comparison for $MoS_2$ nanoribbons and flake for rotated samples. The samples were rotated at two different orientations (0 and 90 degrees) while keeping the same polarization.

# Supplementary Figure 6

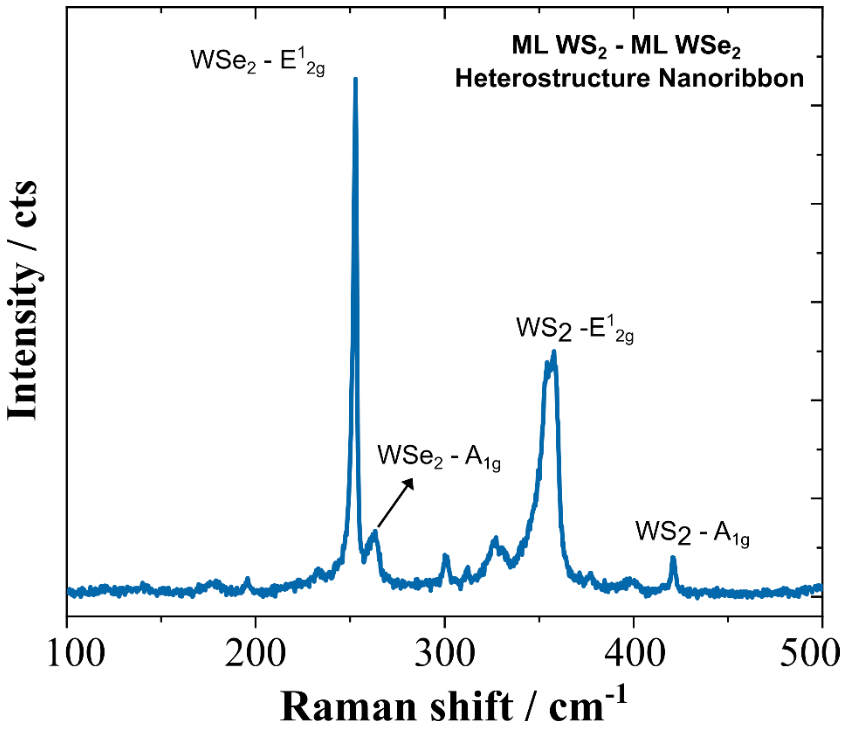


Supplementary Figure 6: Raman spectra for ML $WS_2$ and ML $WSe_2$ heterostructure nanoribbon.

# Supplementary Figure 7

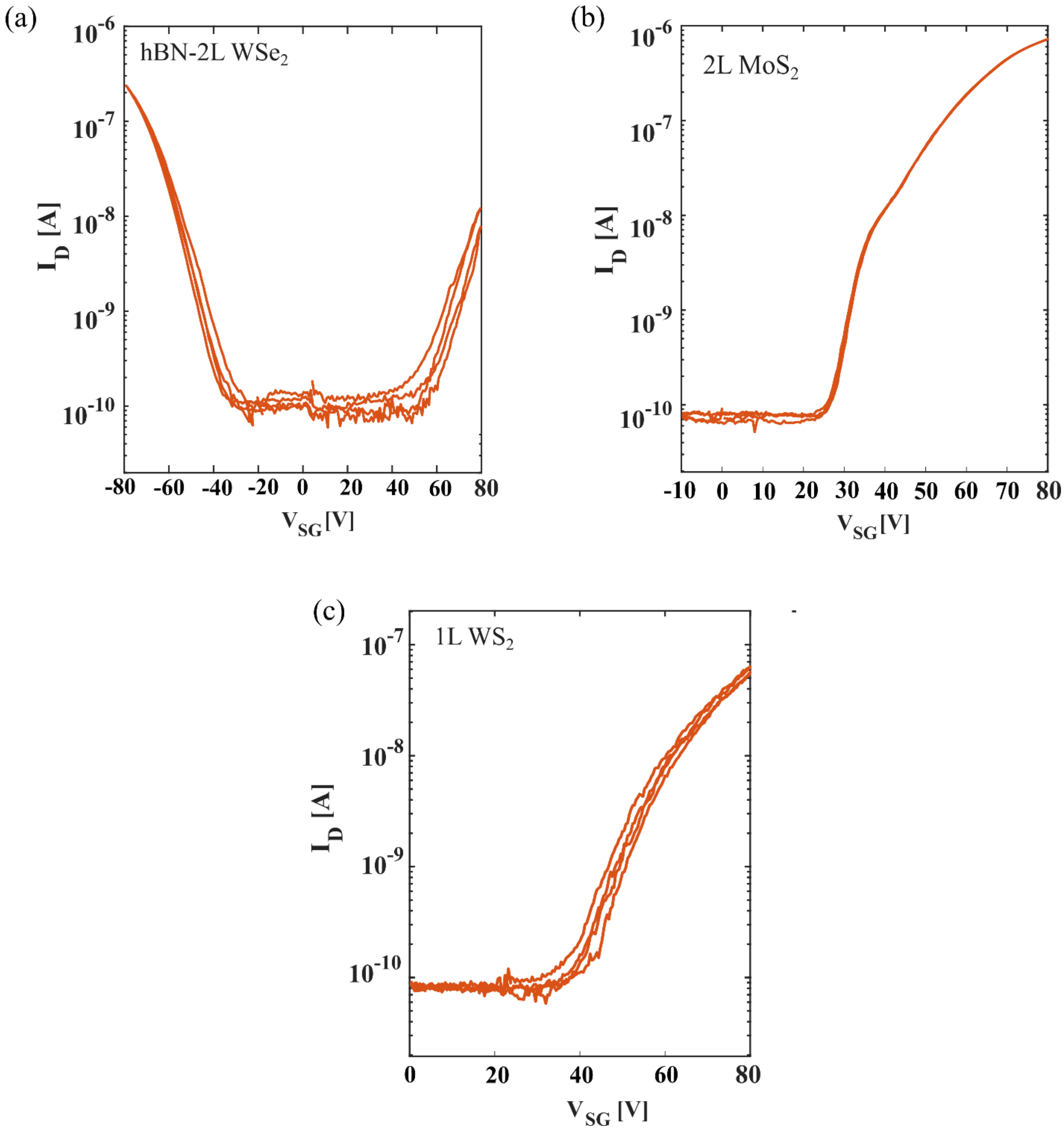


Supplementary Figure 7: (a-c) shows the closure of hysteresis for all TMDC nanoribbons at low temperatures (77K).

# Supplementary Figure 8

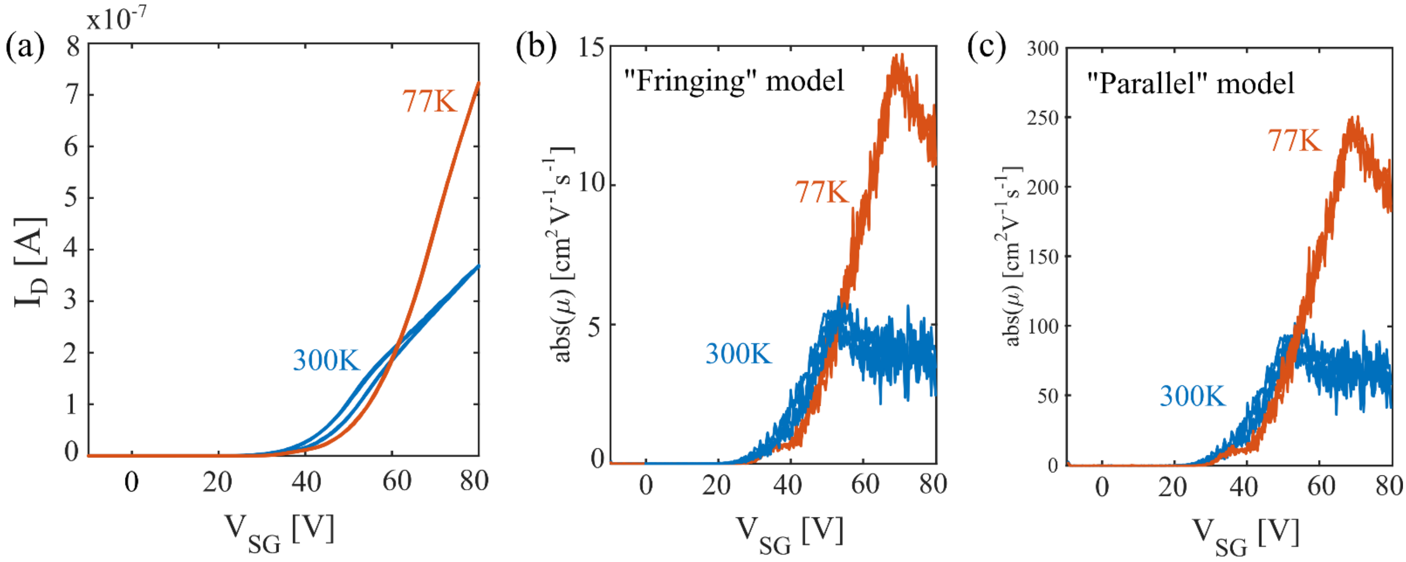


Supplementary Figure 8: (a) Linear source-drain currents ($I_{SD}$) for $MoS_2$ nanoribbons show a significant increase at 77K. (b,c) show increased mobilities for $MoS_2$ nanoribbons at 77K.

# Supplementary Figure 9

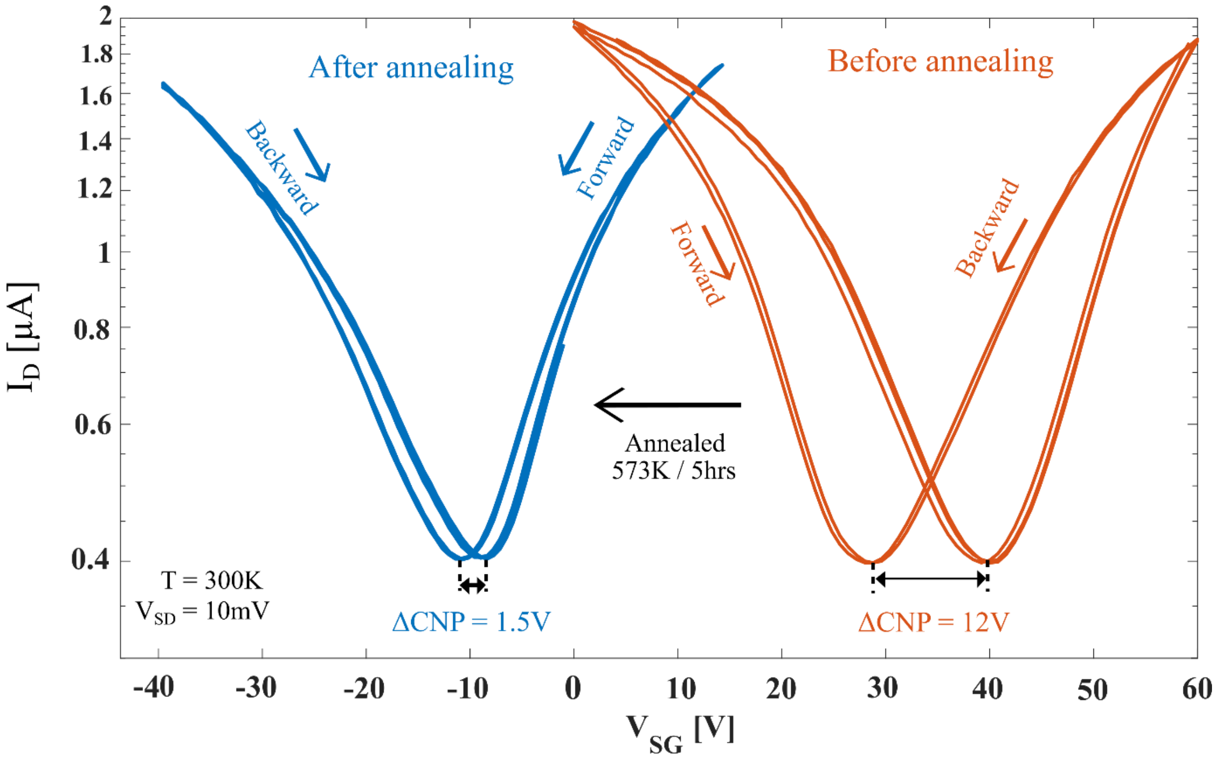


**Supplementary Figure 9**: The effect of annealing on the hysteresis in the electrical transfer curves of graphene NRN-FETs (semi-log scale). The hysteresis is reduced to 1.5 V (annealed) from 12 V (non-annealed). This large reduction in ΔCNP indicates the removal of water molecules from the graphene nanoribbon edges. Mind, the curves are measured at 300 K before and after annealing of the device in low vacuum ($8 \times 10^{-3}$ mbar) and without breaking the vacuum.

# Supplementary Table 2

| 2D material nanoribbon device | Total number of devices made | Working devices | Reason for not working |
|---|---|---|---|
| Graphene | 61 | 48 | 3 – long channels >20 μm, with lacking percolation of the self-assembled organic nanostructures<br><br>10 – unstable/defective $SiO_2$ back gate |
| $MoS_2$ | 28 | 24 | 4 – unstable/defective $SiO_2$ back gate |
| $WS_2$ | 7 | 7 | - |
| $WSe_2$ | 9 | 9 | - |

**Supplementary Table 2:** yield of the fabricated devices, indicating the reasons observed for the device failure.

# Supplementary Figure 10

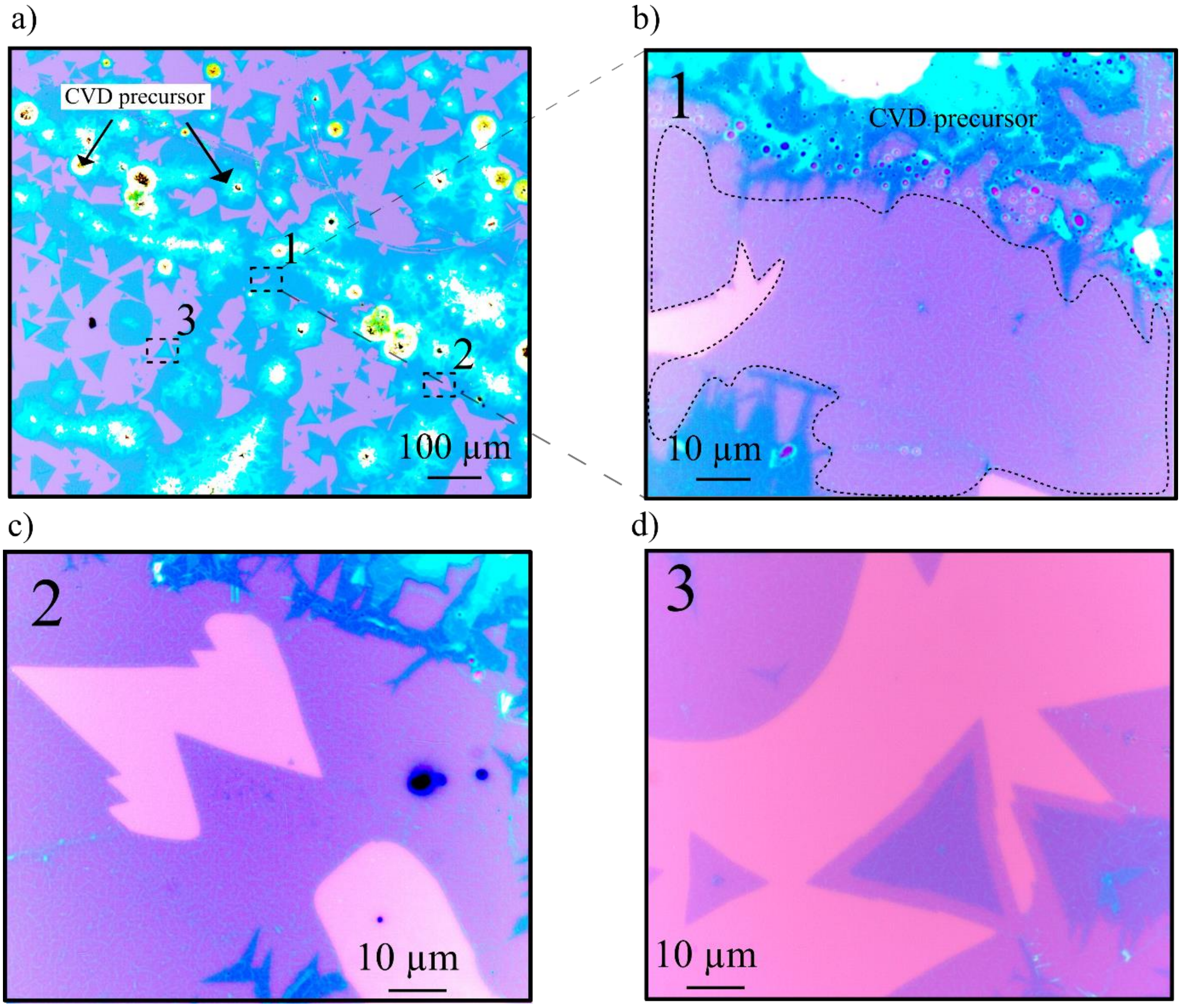


Supplementary Figure 10: Optical images depicting the yield of the nanostructure growth on CVD grown $MoS_2$. (a) large area image of CVD $MoS_2$ which has been exposed to organic nanostructure growth. (b-d) show higher magnification images of three different regions. (b) Dotted boundary region marks the area of monolayer MoS2 covered with organic nanostructures. All areas have excellent coverage of organic nanostructures.

## Supplementary Figure 11

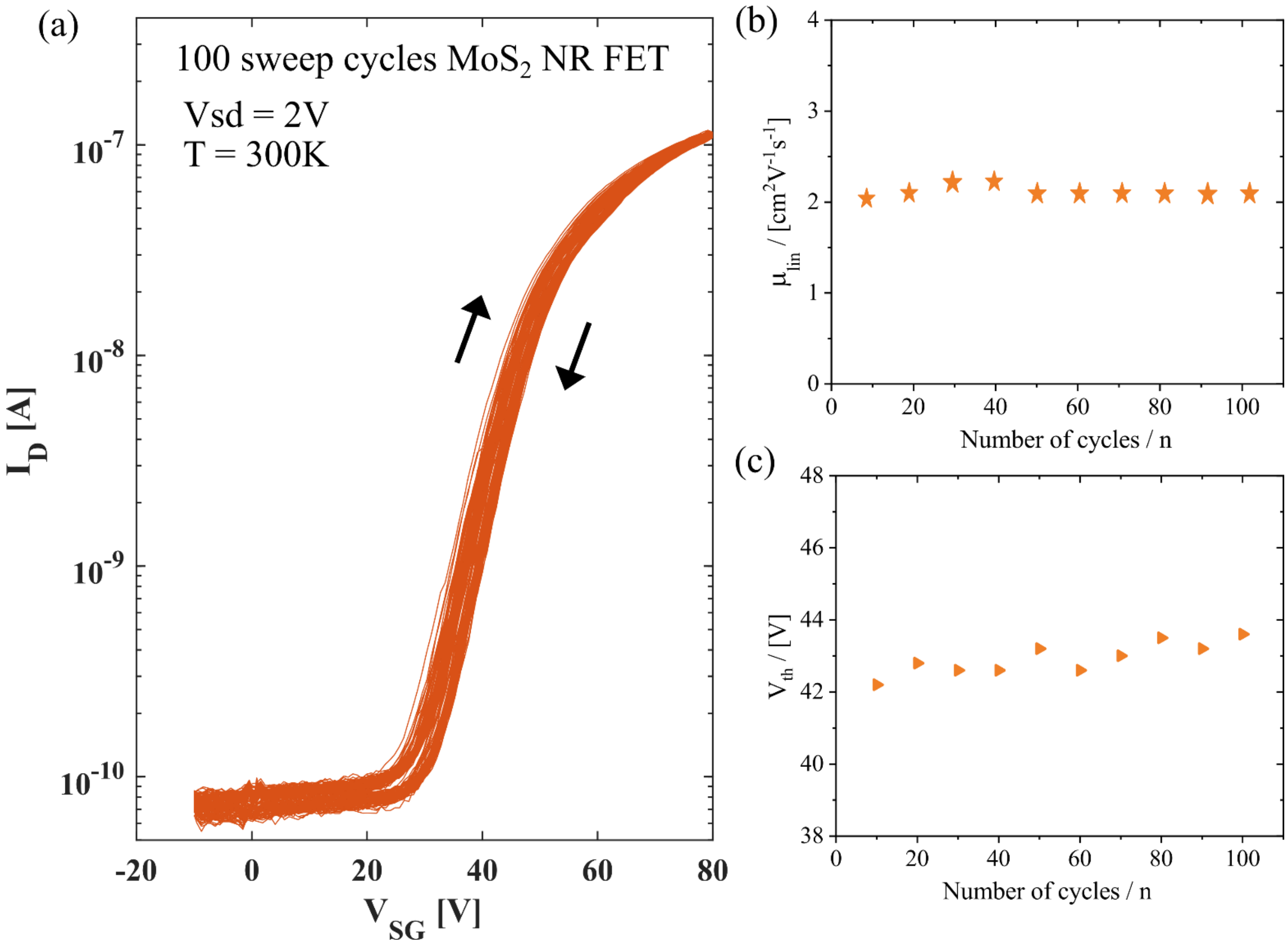


Supplementary Figure 11: the stability of nanoribbons for 100 sweeping cycles. (a) superimposed 100 subsequent forward and backward sweeping electrical transfer curves (semi log scale) of a $MoS_2$ NRN-FET measured under low vacuum ($02\cdot10^{-2}$ mbar) and with 2 $Vs^{-1}$ sweeping rates. (b) statistics for the extracted apparent linear electron mobility ($\mu_{lin}$) as a function of the number of sweeps, considering the fringing capacitance model. (c) statistics of the extracted threshold voltage ($V_{th}$) as a function of the number of sweeps.

### References


[S1] Abramova, V., Slesarev, A. S., & Tour, J. M. Meniscus-mask lithography for narrow graphene nanoribbons. *ACS Nano*, ***7***, 6894-6898 (2013).

[S2] Liu, C. et al. Highly stretchable graphene nanoribbon springs by programmable nanowire lithography. *npj 2D Mater. Appl.*, ***3***, 1-9 (2019).

[S3] Wang, X., & Dai, H. Etching and narrowing of graphene from the edges. *Nat. Chem.*, ***2***, 661-665 (2010).

[S4] Jiao, L., Zhang, L., Wang, X., Diankov, G., & Dai, H. Narrow graphene nanoribbons from carbon nanotubes. *Nature*, ***458***, 877-880 (2009).

.

[S5] Jiao, L., Wang, X., Diankov, G., Wang, H., & Dai, H. Facile synthesis of high-quality graphene nanoribbons. *Nat. Nanotechnol.*, ***5***, 321-325 (2010).

[S6] Vo, T. H. et al. Large-scale solution synthesis of narrow graphene nanoribbons. *Nat. Commun.*, ***5***, 1-8 (2014).

[S7] Cai, J.  et al. Graphene nanoribbon heterojunctions. *Nat. Nanotechnol.*, *9* , 896-900 (2014).

[S8] Barone, V., Hod, O., & Scuseria, G. E. Electronic structure and stability of semiconducting graphene nanoribbons. *Nano Lett.*, ***6***, 2748-2754 (2006).